Electronic structure of MnSb

R. Coehoorn and C. Haas

Laboratory of Inorganic Chemistry, Materials Science Centre, University of Groningen,
Nijenborgh 16, 9747 AG Groningen, The Netherlands

R. A. de Groot

Research Institute for Materials, Faculty of Science, Toernooiveld, 6525 ED Nijmegen, The Netherlands
(Received 18 June 1984)

Self-consistent, spin-polarized energy-band calculations have been performed for MnSb, for both ferromagnetic and antiferromagnetic spin alignments. For ferromagnetic MnSb we find a $3d^{5.5}$ configuration on the Mn atom, with a magnetic moment of $3.3\mu_B$ on the Mn sites, and $-0.06\mu_B$ on the Sb sites. The charge transfer of Mn to Sb is very small. A detailed analysis is made of the strong covalent Mn-Mn and Mn-Sb interactions. The coupling between the moments is described in terms of covalent interactions of unoccupied states of the Sb $5p$ band with the Mn $3d$ bands. These interactions stabilize the ferromagnetic alignment. The calculated spin density, which agrees very well with experimental data, can be easily understood in terms of a model of covalent bonding. We compare the calculated Fermi surface, total density of states, and joint density of states with results of transport measurements, x-ray photoelectron spectroscopy, and optical measurements, respectively.

I. INTRODUCTION

In this paper we present the results of an *ab initio*, self-consistent spin-polarized band-structure calculation of MnSb. The obtained electronic structure is compared with observed physical properties and is used to determine the nature of the magnetic moments and the mechanism of exchange interactions in MnSb.

The first-row transition-metal antimonides which all have the NiAs structure, show a large variety of magnetic properties. While MnSb is the only ferromagnetic compound, CrSb, FeSb, and CoSb are antiferromagnetic, TiSb is paramagnetic and NiSb is diamagnetic.[1] MnSb is a ferromagnetic metal with a Curie temperature of $T_c = 585$ K. The compound has a strong uniaxial magnetic anisotropy; the spontaneous magnetization changes its orientation as a function of the temperature.[2-4]

Two recent investigations of Mn- and Sb-containing Heusler alloys have stimulated our interest in MnSb. From results of a spin-polarized band-structure calculation of NiMnSb, it follows that this material is a so-called "half-metallic ferromagnet."[5] The majority-spin electrons are metallic, while the minority-spin electrons are semiconducting. For the related compound PtMnSb it was reported[6] that the polar Kerr effect—the rotation of the polarization of linearly polarized light by normal reflection at the surface of a ferromagnetic metal—is unusually high. For light with a wavelength of 720 nm, a rotation of $-1.27°$ is found. This is the highest rotation ever found for a metallic material at room temperature. Until this discovery, MnBi, which has the same crystal structure as MnSb, had the highest known Kerr rotation at room temperature, $-0.70°$ at 633 nm. The maximum Kerr rotation of MnSb is a factor of 2 lower.[7] The magneto-optical Kerr effect has some possible technological importance for readout of erasable magnetically stored

information. The manganese pnictides MnAs, MnSb, and MnBi are suitable materials for a quantitative study of the Kerr effect, provided their electronic structures are known.

Several models have been proposed for the electronic structure of the manganese pnictides, particularly for MnSb. The ionic models of Goodenough[8] and Albers and Haas[9] [Figs. 1(a) and 1(b)], in which Mn essentially has four d electrons, are extensions of the common description of the electronic structure of transition-metal halides, sulfides, and oxides.[8] Bärner[10] has proposed an ionic model for the electronic structure of MnAs which was very similar to the model of Goodenough. Results of zero-field nuclear magnetic resonance (Bouwma and Haas[11]), x-ray photoelectron spectroscopy (XPS) (Liang and Chen[12]), optical and transport measurements (Chen et al.[13] and Allen et al.[14]), on the other hand, favor an alloylike band model for the electronic structure. In this band model Mn has a $d^{6.5}$ configuration [Fig. 1(c)], which explains the observed magnetic moment of $3.5\mu_B$ per Mn atom. Both the ioniclike and alloylike models imply a high Mn $3d$ density of states at the Fermi level; however, the observed electronic contribution to the specific heat is
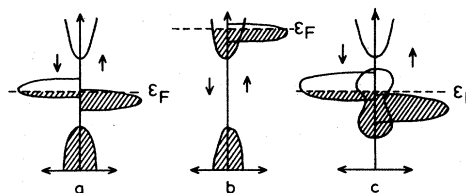

FIG. 1. Schematic representation of the density of states based on models of (a) Goodenough (Ref. 8); (b) Albers and Haas (Ref. 9); (c) Chen et al. (Ref. 13) and Allen et al. (Ref. 14).

relatively low[13] (see Sec. IV).

Band-structure calculations of MnAs and MnSb by Sandratskii *et al.*[15,16] have solved this problem. Their results show that the hybridization between the Mn $3d$ and Sb $5p$ states plays an important role in the electronic structure of these compounds. A calculation of the spin-polarized density of states by Podloucky[17] further confirms their results. These calculations predict a low density of states (DOS) at the Fermi level, which explains the low electronic contribution to the specific heat. Although the calculations of Sandratskii *et al.* were not completely self-consistent, they give a correct picture of the band structure of MnAs and MnSb. In the case of MnAs, the potential was calculated from the configurations $Mn(3d^n4s^{7-n})$-$As(4p^3)$ with the constraint $n^\uparrow - n^\downarrow = m$. Here m is the observed magnetic moment of $3.4\mu_B$, while $n^\uparrow$ and $n^\downarrow$ are the number of d electrons with majority and minority spins, respectively. This means that in the self-consistent procedure, the only free parameter was n, the total number of d electrons. For MnSb they used the configuration $Mn(3d^{5.3}4s^{1.7})$, which was found to give a self-consistent number of d electrons for MnAs. Because the experimental value of m is used, the calculation just mentioned lacks complete self-consistency. We have therefore performed fully self-consistent *ab initio* band-structure calculations for ferromagnetic and antiferromagnetic MnSb.

We have used the obtained band-structure of MnSb, and in particular the orbital composition of the wave functions, for a detailed discussion of two fundamental problems in the magnetism of metallic transition-metal compounds, viz., the nature of the magnetic moments and the mechanism of the exchange interaction between these moments.

Several models have been proposed for the magnetic properties of metallic solids. In the Stoner model of band magnetism, the electrons and the magnetic moments are delocalized, and the exchange splitting of the energy bands below T_c leads to the ferromagnetic properties.[18,19] This band model of magnetism has been applied to transition metals, and in particular to weakly magnetic compounds such as $ZrZn_2$. A drawback of the band model of magnetism is that it fails to give an adequate description of the magnetic properties above T_c.

In the Heisenberg model one assumes the presence of localized electrons and local magnetic moments, as a result of strong correlations between the electrons.[18] The localized magnetic moments are ordered below T_c and disordered above T_c. This description has also been applied to transition metals, and it is valid in particular for the strongly localized magnetic moments of the rare-earth metals.

The nature of magnetic moments in strongly covalent transition-metal compounds such as the Heusler alloys has been discussed recently by Kübler *et al.*[20,21] These authors find that the electrons are delocalized, but the magnetic moments are strongly localized on the transition-metal atoms. An interesting point is that in MnSb the nearest-neighbor Mn—Mn distance ($d = 2.88$ Å) is in between the nearest-neighbor distance in the Heusler alloys (e.g., Pd_2MnSb, $d = 6.34$ Å) and in pure Mn, ($d = 2.24$ Å). From our band-structure calculation we find also in MnSb itinerant electrons and magnetic moments localized on the Mn atoms.

There exist several contributions to the exchange interaction between magnetic moments in transition-metal compounds.[8,18] First, there is a direct exchange interaction due to overlap of d orbitals of the magnetic atoms. Second, we mention the superexchange interaction via a hybridization of metal d orbitals with orbitals of the nonmagnetic atoms; this mechanism operates also in insulating crystals. Finally, in metallic materials there is a contribution of indirect exchange via conduction electrons (or holes) in a partly occupied energy band. In a simple system with localized moments interacting with electrons in a free-electron-like band, this leads to a Ruderman-Kittel-Kasuya-Yoshida—type interaction, which is long range and oscillating with distance.[18] If the Fermi surface is not free-electron-like, and if strong hybridization between conduction electrons and magnetic electrons occurs, the situation is more complicated and this indirect interaction cannot be separated from the superexchange contribution. In this paper we give a discussion of the exchange interactions in MnSb, based on a comparison of the calculated band structures of a ferromagnetic and an assumed antiferromagnetic state of MnSb. In particular it was possible from a detailed consideration of the orbital composition of the wave functions to trace the different contributions to the exchange. Finally we used the calculated band structure to provide a framework for the interpretation of the observed physical properties.

Section II of this paper gives the details of the calculations of the band structure. In Sec. III, the energy bands and the densities of states are presented, and the d-p hybridization between Mn and Sb and the competition between ferromagnetism and antiferromagnetism is discussed. In Sec. IV the results of the calculations are compared with experimental data on XPS, magnetization, spin-polarized neutron diffraction, optical and specific heat measurements. Section V contains the concluding remarks.

II. DETAILS OF THE CALCULATION

For the band-structure calculations the augmented spherical wave (ASW) method of Williams, Kübler, and Gelatt was used.[22] Scalar relativistic effects (mass-velocity and Darwin terms) were included as described by Methfessel and Kübler.[23] The local exchange-correlation potential of von Barth and Hedin[24] was used. For the Mn atoms the $3d$, $4s$, and $4p$ functions were used as basis, for the Sb atom the basis consisted of $5s$, $5p$, and $5d$ functions. For each spin direction the order of the secular matrix was 36. Mn $4f$ contributions were included in the internal summation of the three-center contributions to the matrix elements. This can be regarded as treating f states as a perturbation.

From the occupation numbers of the s, p, d, and f states, the charge density within a spherical region—the Wigner-Seitz sphere—around each atom is calculated. This is done by averaging over the m quantum number associated with a certain n,l contribution, so that this procedure leads to a spherical charge density, and the poten-
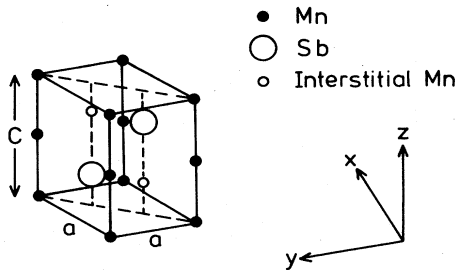
FIG. 2. Hexagonal unit cell of MnSb.

TABLE II. Input parameters for the ASW calculation.

Lattice constants	$a = 4.112$ Å
	$c = 5.740$ Å
c/a ratio	1.396
Wigner-Seitz sphere radii	
Mn	1.563 Å
Sb	1.839 Å
Mn—Mn distances	2.870 Å and 4.112 Å
Sb—Sb distance	3.725 Å
Mn—Sb distance	2.774 Å

tial has also spherical symmetry. In this approximation, crystal-field effects are neglected. Within each iteration step the absolute value of the difference between the input and output charge densities for each of the atoms is integrated over the Wigner-Seitz (WS) sphere:

$$\Delta Q = \int_{WS\ sphere} |\rho_{out}(\vec{r}) - \rho_{in}(\vec{r})|\, d\vec{r} . \tag{1}$$

The self-consistency criterion was that ΔQ should be lower than 10^{-5}, which was realized after 12 iteration steps starting from atomic potentials. The convergence of the bands was better than 1 meV. The only input parameters were the atomic numbers, the crystal structure and the Wigner-Seitz radii.

MnSb crystallizes in the hexagonal NiAs structure, space group $P6_3/mmc\text{-}D_{6h}^4$ (No. 194 in the *International Tables for X-ray Crystallography*). The unit cell is shown in Fig. 2. It consists of two Mn atoms at the $2a$ sites $(0,0,0)$ and $(0,0,\frac{1}{2}c)$ and two Sb atoms at the $2c$ sites $(\frac{1}{3}a\sqrt{3},0,\frac{1}{4}c)$ and $(\frac{1}{6}a\sqrt{3},-\frac{1}{2}a,\frac{3}{4}c)$ in a Cartesian coordinate frame. The Mn atoms are coordinated by a trigonally distorted octahedron of Sb atoms. The Mn atoms form trigonal prisms around the Sb atoms.

The experimental lattice parameters are tabulated in Table I. The lattice parameters and Wigner-Seitz radii which were used can be found in Table II. The sum of the Wigner-Seitz sphere volumes equals the volume of the unit cell. The c/a ratio was chosen to be equal to the measured value at a temperature of 4 K (Table I), while the length of the a axis was taken to be somewhat lower than the experimental value, in order to minimize the total energy.

In nonstoichiometric $Mn_{1+x}Sb$ excess Mn atoms are accommodated in the interstitial trigonal-bipyramidal holes in the hexagonal packing of Sb atoms (see Fig. 2). The Mn atoms form a trigonal prism around the interstitial atom.

III. RESULTS OF THE CALCULATION

A. Ferromagnetic MnSb

The calculated energy bands for both spin directions along symmetry lines in the hexagonal Brillouin zone (Fig. 3) are plotted in Fig. 4. We have used the symmetry notations of Miller and Love.[27] The differences between their symmetry labels and those of Herring[28] are tabulated in Table III. The combinations of atomic s, p, and d functions which transform according to the irreducible representations of the group of the wave vector have been tabulated by Tylor and Fry.[29] The symmetry labels show which bands are coupled by the crystal Hamiltonian, forming hybridized states.

The total density of states (Fig. 5) and the density of states decomposed by atom and l contribution (Fig. 6 and 7) were derived from the band energies in 1000 points on a regular mesh in the $\frac{1}{24}$ Brillouin zone, using energy intervals of 0.1 eV. The partial-DOS plots give a quick insight in the wave-function character of the bands. More quantitative information is given in the Tables IV and V, which give the contributions of the basis functions to the wave functions at Γ for the two spin directions. The numbers of s, p, d, and f electrons per spin direction and the partial DOS at the Fermi level for Mn and Sb are tabulated in Table VI. One must bear in mind that in a solid, the number of electrons per atom and the partial densities of states are not uniquely defined, but depend on the atomic radii chosen (Table II).

The band structure shows an exchange splitting of the Mn $3d$ band of about 3.5 eV. For the majority-spin direc-

TABLE I. Experimental lattice parameters MnSb.

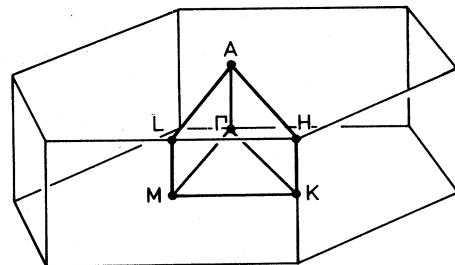| Method	a (Å)	c (Å)	c/a
X-ray diffraction 300 K[a]	4.120	5.784	1.403
X-ray diffraction 300 K[b]	4.13	5.79	1.402
Neutron diffraction 4.2 K[b]	4.1220 (3)	5.7549 (4)	1.396

[a]Reference 25.
[b]Reference 26.

FIG. 3. First Brillouin zone of the hexagonal lattice showing the position of high symmetry points and lines.

FIG. 4. Energy band structure of MnSb for (a) majority-spin and (b) minority-spin electrons. Ferromagnetic spin alignment.

tion there is a 2-eV-wide peak in the DOS around −2.5 eV, which originates from states with Mn $3d$ character. The corresponding bands have little dispersion in the ΓM and ΓK directions, but are more dispersive in the ΓA direction. Due to hybridization with the states in the underlying broad Sb $5p$ band, there is a tail in the Mn $3d$ partial DOS which extends to the region above the Fermi

TABLE III. Differences between symmetry notation of Miller and Love (Ref. 27) and Herring (Ref. 28) for the space group D_{6h}^4. For points Γ, L, and A the notations are identical.

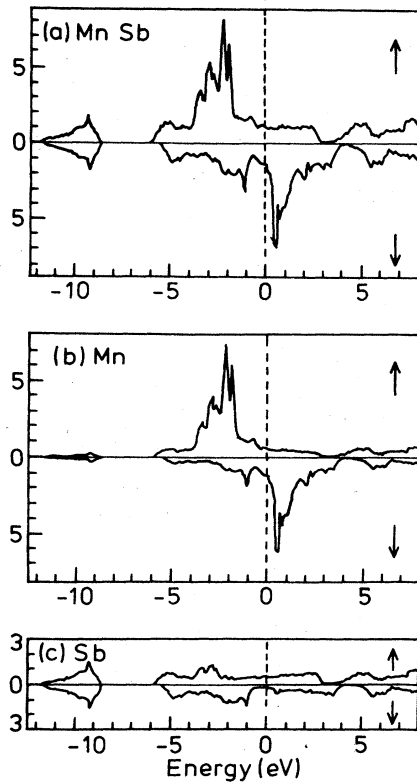| Miller and Love	M_4^+	M_4^-	M_2^+	M_2^-	K_3	K_4	H_1	H_3
Herring	M_2^+	M_2^-	M_4^+	M_4^-	K_4	K_3	H_3	H_1

FIG. 5. (a) Total density of states of F-MnSb, (b) partial Mn density of states, (c) partial Sb density of states. Units: states eV^{-1}(unit cell)$^{-1}$.

level. A similar situation is found for the minority-spin direction. In this case we find a Mn $3d$ peak in the DOS at about 1 eV above the Fermi level, with a tail in the partial DOS which extends to energies below the Fermi level.
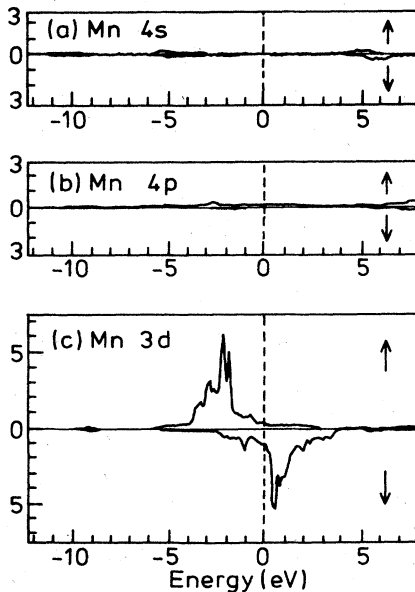

FIG. 6. Angular momentum and spin-decomposed density of states for F-MnSb. Contribution of Mn. Units: states eV^{-1}(unit cell)$^{-1}$.
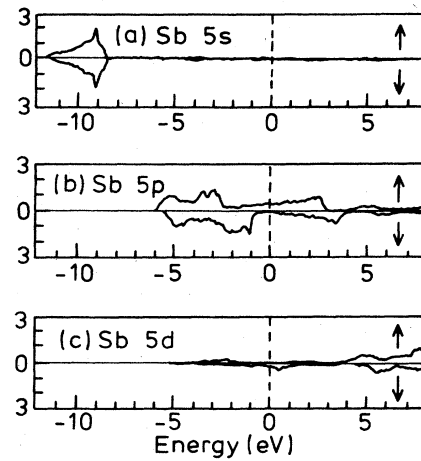

FIG. 7. Angular momentum and spin-decomposed density of states for F-MnSb. Contribution of Sb. Units: states eV^{-1}(unit cell)$^{-1}$.

Because of this hybridization the calculated magnetic moment per Mn atom is not $5\mu_B$, but only 3.24 μ_B (Table VI).

The Sb partial DOS consists of three major parts.

(1) The Sb $5s$ band, 10 eV below the Fermi level, with a width of about 3 eV.

(2) The Sb $5p$ band, from -5.7 to $+3.0$ eV for majority-spin electrons and from -5.3 to $+4.0$ eV for minority-spin electrons. Due to the hybridization with Mn $3d$ states, a small net magnetic moment of $-0.06\,\mu_B$ per Sb atom results.

(3) The Sb $5d$ band, strongly mixed with Mn $4s$ and $4p$ states, at energies above 4.0 eV.

The pronounced structure in the Sb $5p$ partial DOS shows that the p-d hybridization cannot be described simply as an interaction of Mn $3d$ states with a structureless continuum of free-electron-like Sb-derived states. Furthermore, we cannot give a single value for the exchange splitting of the Sb $5p$ band, as the p-d interaction depends on the symmetry properties of the bands.

We will discuss the hybridization mechanism by analyzing in some detail the band structure of Γ. The Sb $5p$ band contains six p states per unit cell, which can be classified as

$$\Gamma_3^+:\ z_1 + z_2\ ,$$
$$\Gamma_6^-:\ x_1 + x_2 \pm i\,(y_1 + y_2)\ ,$$
$$\Gamma_5^+:\ x_1 - x_2 \pm i\,(y_1 - y_2)\ , \tag{2}$$
$$\Gamma_2^-:\ z_1 - z_2\ .$$

We have taken x, y, and z as shorthand notations for p_x, p_y, and p_z orbitals. Subscripts 1 and 2 refer to the two antimony sites. If we do not take into account the hybridization with Sb $5p$ states, the shape of the Mn $3d$ band is determined by the interaction between states on atoms along the c axis. This is because the nearest-neighbor

TABLE IV. Contributions from the basis functions to the wave functions at Γ for ferromagnetic MnSb. Majority-spin direction. The tabulated numbers are the squares of the absolute values of the coefficients, summed over equal atoms, and expressed in percents. Only contributions larger than 1% are tabulated.

| Majority-spin | | Mn | | | | | | | | | Sb | | | | | | | | |
Energy (eV)	Symmetry	s	y	z	x	xy	yz	z^2	xz	x^2-y^2	s	y	z	x	xy	yz	z^2	xz	x^2-y^2
-11.69	1^+	43									57								
-8.70	4^-			29							63						8		
-5.70	3^+	19						27					53						
-3.68	5^+					57	26		26	57		17		17					
-3.21	1^+							97											
-2.73	5^+					29	68		68	29					3				3
-2.34	6^+					97				97						3		3	
-1.74	6^+						100		100										
-0.52	3^+	7						72					21						
0.92	6^-		21		21							74		74	5				5
2.21	5^+					15	3		3	15		79		79	3				3
2.75	2^-			3									96						
3.60	4^-			20							31						49		

TABLE V. Contributions from the basis functions to the wave functions at Γ. Ferromagnetic MnSb, minority-spin direction. Only contributions larger than 1% are tabulated.

Minority-Spin		Mn									Sb								
Energy (eV)	Symmetry	s	y	z	x	xy	yz	z^2	xz	x^2-y^2	s	y	z	x	xy	yz	z^2	xz	x^2-y^2
−11.58	1^+	41									59								
−8.68	4^-			28							64								
−5.28	3^+	19											60				8		
−2.20	5^+					48	16	20				36		36					
−0.79	1^+	2						94	16	48							3		
−0.25	5^+					20	74		74	20					6				6
+0.28	6^+				18	93				93						6		6	
1.10	6^-		18					80				78		78					
1.17	6^+						100		100										
2.37	3^+	4											16						
2.74	2^-			3									97						
3.72	5^+					32	5		5	32		60		60	3				
3.96	4^-			17							28						55		3

TABLE VI. Numbers of s, p, d, and f electrons per unit cell, partial DOS $N(\epsilon_F)$ at the Fermi level, and magnetic moments. There are two formula units MnSb per unit cell.

		Number of electrons		$N(\epsilon_F)$ in states eV^{-1}(unit cell)$^{-1}$	
		↑	↓	↑	↓
Mn	$4s$	0.59	0.50	0.035	0.010
	$4p$	0.70	0.65	0.111	0.020
	$3d$	8.72	2.29	0.493	1.140
	$4f$	0.06	0.05	0.016	0.006
Sb	$5s$	1.73	1.71	0.063	0.001
	$5p$	2.82	3.20	0.402	0.053
	$5d$	0.44	0.30	0.054	0.125
	$4f$	0.18	0.06	0.022	0.023
Total		15.24	8.76	1.196	1.432

Total number of valence electrons: $n^\uparrow + n^\downarrow = 24.0$ per unit cell

Magnetic moment per Mn atom: $\frac{1}{2}(n^\uparrow - n^\downarrow) = 3.24\mu_B$

Magnetic moment on Mn site: $3.30\ \mu_B$

Magnetic moment on Sb site: $-0.06\ \mu_B$

Total DOS at Fermi level: $N(\epsilon_F) = 2.63$ states eV^{-1}(unit cell)$^{-1}$

Charge transfer to Sb: 0.22 electrons per Sb atom

Mn-Mn distance along the c axis (2.87 Å) is much smaller than the distance of Mn atoms in the x-y plane (4.12 Å). There are ten d states per unit cell per spin direction, which can be classified as

$$\Gamma_1^+\ a_{1+}^T:\ z_1^2 + z_2^2\ ,$$

$$\Gamma_5^+\ e_+:\ yz_1 - yz_2 \pm i(xz_1 - xz_2)\ ,$$

$$\Gamma_5^+\ e_+^T:\ xy_1 + xy_2 \pm i[(x^2 - y^2)_1 + (x^2 - y^2)_2]\ ,$$

$$\Gamma_6^+\ e_-^T:\ xy_1 - xy_2 \pm i[(x^2 - y^2)_1 - (x^2 - y^2)_2]\ ,$$

$$\Gamma_6^+\ e_-:\ yz_1 + yz_2 \pm i(xz_1 + xz_2)\ ,$$

$$\Gamma_3^+\ a_{1-}^T:\ z_1^2 - z_2^2\ .$$

(3)

Here we have used z^2, xy, yz, xz, and $(x^2 - y^2)$ as shorthand notations for $d_{3z^2-r^2}$, d_{xy}, d_{yz}, d_{xz}, and $d_{x^2-y^2}$ orbitals. Subscript 1 and 2 refer to the two Mn sites. The notations a_1^T, e, and e^T, with $+$ and $-$ signs for bonding and antibonding states, respectively, have been introduced by Goodenough.[30]

We have analyzed the hybridization with a simple model. The hybridization of the Sb $5p$ and Mn $3d$ orbitals is described by σ bonding interactions of Mn $3d$ e_g-type orbitals with Sb $5p$; π-bonding interactions of Mn $3d$ e_g^t and Mn a_{1g}^t orbitals with Sb $5p$ are neglected. We assume that the splitting into bonding and antibonding levels is symmetric; this is the case if the overlap integrals between the orbitals are zero. From our calculated energy
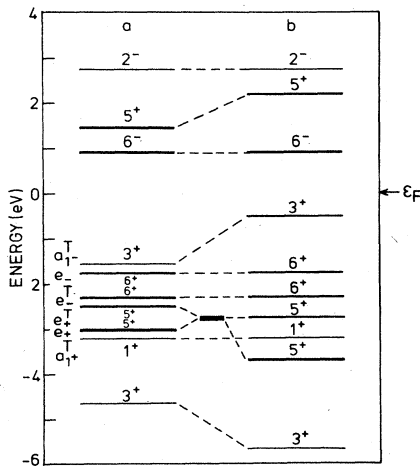

FIG. 8. Analysis of the hybridization mechanism for ferromagnetic MnSb at the Γ point. Majority-spin electrons. (a) Energy levels in the absence of p-d hybridization. (b) Calculated energy levels. Heavy lines are degenerate states.
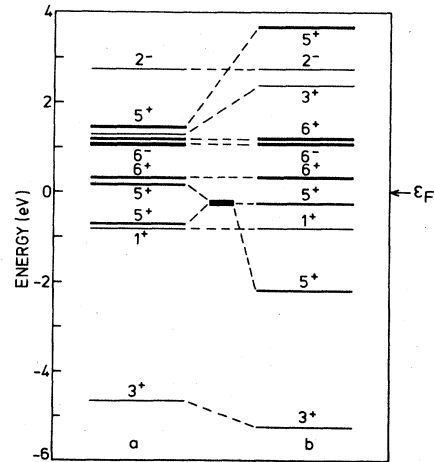

FIG. 9. Analysis of the hybridization mechanism for ferromagnetic MnSb at the Γ point. Minority-spin electrons. (a) Energy levels in the absence of p-d hybridization. (b) Calculated energy levels. Heavy lines are degenerate states.

levels we can then derive the position of the levels which would be found in the absence of p-d hybridization. The result is shown in Fig. 8 for the majority-spin direction and in Fig. 9 for the minority-spin direction. The left part of these diagrams gives the position of Mn $3d$ and Sb $5p$ states in the absence of p-d hybridization, the right part gives the calculated energies. The character of the wave functions of these levels is given in Tables IV and V. We have constructed these diagrams in the following way.

(1) Mn $3d$ states have positive parity, which implies that Γ_2^- and Γ_6^- states play no role in the p-d interaction. The same is true for Γ_6^+ manganese states, because there is no antimony Γ_6^+ state. Therefore the Γ_2^- and Γ_6^- states will have the same energy for the two spin directions.

(2) Both Mn Γ_5^+ states can hybridize with the Sb Γ_5^+ state. The manganese states can combine to states with e_g^t and e_g symmetry, of which only e_g states interact appreciably with the antimony states. Only this e_g state forms a σ-bonding and antibonding combination with the Sb Γ_5^+ state. The interaction is strongest for the minority-spin electrons, because of the smaller energy distance between the interacting states.

(3) From the energy distance between e_-^T and e_- states and the energy of the $\Gamma_5^+(e_g^t)$ state, the position of the e_+ and e_+^T states has been derived.

(4) From the energy distance between the $\Gamma_1^+(a_{1+}^T)$ state, which does not hybridize with Sb $5p$ states, and the $\Gamma_5^+(e_+)$ state, we can derive the position of the $\Gamma_3^+(a_{1-}^T)$ state.

(5) The position of Sb $5p$ Γ_5^+ and Γ_3^+ states, without p-d hybridization, can be derived by assuming that the mean energy of states that form bonding and antibonding combinations does not change. This is indeed the case if the overlap integral of the two orbitals is zero.

By this construction we find that the bonding-antibonding splitting of Mn $3d$ states increases in the order e^T, e, a_1^T being nearly the same for e and a_1^T states. The fact that the splitting of e^T states is small can be easily understood from the shape of the xy and x^2-y^2 orbitals. The same result is found by Tyler and Fry for $3d$ states in NiS.[29] Without p-d hybridization the width of the d band is mainly due to d-d overlap along the c axis. We find widths of 1.7 and 2.1 eV for majority- and minority-spin electrons, respectively.

Minority-spin electrons are somewhat more delocalized than the majority-spin electrons. The intra-atomic exchange contribution to the splitting of the d bands is 2.7 eV, which is 0.8 eV smaller than the total splitting of the d peaks (Fig. 6, peak positions at -2.5 and $+1.0$ eV). This difference is caused by d-p hybridization between Γ_5^+ states, which is more pronounced for minority-spin states. The lower part of the d band for minority-spin electrons is smeared out and is shifted to lower energy. The hybridized Mn d—Sb p states are clearly seen as peaks in the partial Sb $5p$ density of states at -3.1 and -1.5 eV for majority- and minority-spin directions.

With Sandratskii et al.,[16] we conclude that p-d hybridization plays an important role in the electronic structure of MnSb. The electronic configuration (Mn $d^{5.3}s^{1.7}$)

which they used is close to the final result (Mn $d^{5.5}s^{0.6}p^{0.7}$) of our self-consistent calculation. The main features, such as the total width of the Sb $5p$ band, the distance between majority- and minority-spin Mn $3d$ bands, and the position of most of the bands at Γ, agree very well. A major difference is that Sandratskii et al. find that the Mn $3d$ peaks in the DOS consists of two (majority-spin) and three (minority-spin) clearly separated peaks, while the structure of our d bands is less pronounced.

We make a final remark about the spin-orbit interaction. An indication of the spin-orbit interaction strength we can expect for MnSb is given by the observed splittings between Sb $p_{1/2}$— and Sb $p_{3/2}$—derived states at Γ in the valence band of InSb and GaSb which are 0.82 and 0.80 eV, respectively.[31] A similar value is also obtained from atomic spectra.[32] In order to estimate the effect of spin-orbit interaction, we have included the operator

$$\lambda \vec{L} \cdot \vec{S} = \lambda (\tfrac{1}{2}[L^+S^- + L^-S^+] + L_z S_z) \tag{4}$$

in the Hamiltonian, operating only on Sb $5p$ states, with an interaction parameter $\lambda = (\tfrac{2}{3}) \times 0.8$ eV, corresponding to an atomic splitting

$$E(p_{3/2}) - E(p_{1/2}) = 0.8 \text{ eV} . \tag{5}$$

The most pronounced effects are found at Γ, where the Sb Γ_6^- and Γ_5^+ states are split by 0.5 eV for the case that the magnetization is oriented parallel to the z axis. The effect on Mn $3d$—derived states depends on their hybridization with Sb $5p$ states, and leads to splittings less than 0.2 eV. The splittings at other points in the Brillouin zone are 0.4, 0.25, 0.1, 0.4, and 0.2 eV at A, M, L, K, and H, respectively. We conclude that inclusion of spin-orbit interaction alters details in the band structure, but that the effect is small compared to the width of the Sb $5p$ band and the intra-atomic exchange splitting on Mn.

B. Competition between ferromagnetism and antiferromagnetism

As will be shown in Sec. IV, the magnetic moments are localized on the Mn sites. The local exchange interaction results in a coupling between moments on different atoms. The foregoing analysis of the band structure suggests that this coupling can be discussed in terms of a direct exchange interaction due to d-d overlap along the c axis, and an indirect exchange interaction due to p-d hybridization.

Quantitative information about the competition between ferromagnetism and antiferromagnetism has been obtained from a band-structure calculation of hypothetical antiferromagnetic MnSb (AF-MnSb). We have used the same lattice constants and Wigner-Seitz radii as in the calculation for ferromagnetic MnSb (F-MnSb, Table II). The magnetic unit cell was assumed to be equal to the crystallographic unit cell (Fig. 2), with the moments on the two manganese sites along the c axis being antiparallel. This magnetic structure with parallel moments in the basal phase and antiparallel orientation of the moments in neighboring planes is observed in MnTe and

CrSb (Ref. 33), which also crystallize in the NiAs structure. The calculated total energy for antiferromagnetic MnSb (AF-MnSb) is 38 meV per unit cell higher than the total energy of F-MnSb, consistent with the observed ferromagnetic alignment. Figure 10 shows spin-up and spin-down Mn $3d$ density of states on one sublattice, and the Sb $5p$ density of states. In Table VII we have compared results of the calculation for AF-MnSb with those for F-MnSb.

Just as in the case of F-MnSb, we have analyzed the band structure at Γ in terms of d-d interactions and d-p interactions (Fig. 11). Since the two Mn atoms in the unit cell are no longer equivalent, the symmetry is lowered to the space group D_{3d}^3. At Γ the relations between symmetry notations in the D_{6h}^4 and the D_{3d}^3 groups are

$$1^+, 3^+ \rightarrow 1^+ ,$$
$$2^-, 4^- \rightarrow 2^- ,$$
$$5^+, 6^+ \rightarrow 3^+ ,$$
$$5^-, 6^- \rightarrow 3^- .$$

(6)

Because of the lower symmetry of the crystal, more states can hybridize. Therefore Table VIII, which gives the contributions from the basis functions to the wave functions at Γ, is of great help in the discussion of the hybridization. We give the analysis for one spin direction. For the other spin direction the contribution from both Mn atoms, labeled 1 and 2 in Table VIII, must be interchanged.

The Γ_3^+ states at -2.5 and $+0.3$ eV are Mn $3d$ states for one spin direction on Mn1 and Mn2, respectively. Table VIII shows that they contain very little d character of the other Mn atom, and no significant Sb p character. Therefore, in the absence of d-p and d-d hybridization, the d levels of Mn1 and Mn2 are situated at about -2.4 and $+0.2$ eV, respectively, if we assume a small repulsion of Mn1 and Mn2 d states of about 0.1 eV due to hybridization effects (direct exchange). These positions coincide with the centers of gravity of the Mn d states for F-MnSb without d-p hybridization for majority-spin [at -2.4 eV, Fig. 8(a)] and minority-spin (at $+0.2$ eV) electrons. This proves quite clearly that the exchange splitting of Mn d states is an intra-atomic effect which is the same for F-
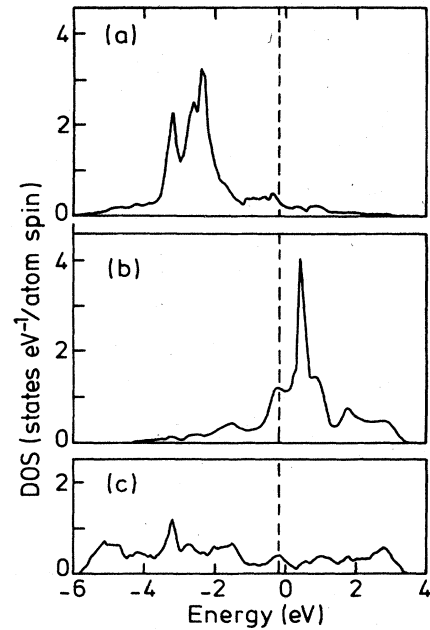

FIG. 10. Density of states of antiferromagnetic MnSb. (a) Sublattice spin-up Mn $3d$ density of states. (b) Mn $3d$ spin-down density of states on the same sublattice. (c) Sb $5p$ density of states (per atom).

MnSb and AF-MnSb. The slightly different number of d electrons in F-MnSb and AF-MnSb (Table VII) has no observable influence on the exchange splitting. The positions of the Sb $5p$ states in the absence of p-d hybridization were taken from the analysis of F-MnSb (Figs. 8 and 9), which completes the construction of Fig. 11(a).

The Mn d_{z^2} states (Γ_1^+) mix with bonding Sb p_z states [Fig. 11(b)] and with each other [Fig. 11(c)]. The estimated energy shift due to interactions between d electrons on neighboring Mn atoms is 0.4 eV for these d_{z^2} states, and 0.1–0.2 eV for the Γ_3^+ states with Mn $3d$ character. Using also the simplifying assumption that states with mainly Sb $5p$ character do not take part in the d-d interactions, Fig. 11(b) is derived from the calculated energy scheme [Fig. 11(c)].

TABLE VII. Results of the band-structure calculation of AF-MnSb, compared to calculated data for F-MnSb. Energies with respect to the Fermi energy of F-MnSb.

	AF-MnSb	F-MnSb
Total magnetic moment (μ_B per Mn atom)	3.16	3.24
Center Mn $3d$ peaks (eV)	-2.7	-2.5
	$+0.3$	$+1.0$
Separation Mn $3d$ peaks (eV)	3.0	3.5
DOS at ϵ_F [states eV^{-1}(unit cell)$^{-1}$]	4.8	2.6
Number of occupied states on one sublattice per unit cell		
Mn $3d\uparrow$	4.27	4.36
Mn $3d\downarrow$	1.22	1.14
Sb $5p\uparrow$	1.50	1.60
Sb $5p\downarrow$	1.50	1.41

TABLE VIII. Contributions from the basis functions to the wave functions at Γ for antiferromagnetic MnSb, in one spin direction. Only contributions larger than 1% are tabulated. Energies are referred to the Fermi level of ferromagnetic MnSb. For antiferromagnetic MnSb the Fermi level is found at -0.15 eV.

Energy (eV)	Symmetry	Mn1									Mn2							
		s	y	z	x	xy	yz	z^2	xz	x^2-y^2	s	z	x	xy	yz	z^2	xz	x^2-y^2
-11.72	1^+	22		14							20							
-8.78	2^-																	
-5.59	1^+	9						17			10	14				9		6
-3.40	3^+					55	17		17	55								
-2.57	1^+	3						70						6		21		
-2.50	3^+					25	69		69	25				1	3		3	1
-0.89	3^+					14	6		6	14				57	3		3	57
$+0.30$	3^+						6		6	4		9	9	10	82		82	10
0.90	3^-		11		11													
1.17	1^+							13			5					66		
2.66	2^-			2		4						1		22				
2.96	3^+													3				
3.69	2^-			10													5	22

Sb1 and Sb2

Energy (eV)	Symmetry	s	y	z	x	xy	yz	z^2	xz	x^2-y^2
-11.72	1^+	58								
-8.78	2^-	63								
-5.59	1^+			56						
-3.40	3^+		17		17					
-2.57	1^+			4						
-2.50	3^+					2				2
-0.89	3^+		14		14		3		3	
$+0.30$	3^+							8		
0.90	3^-		75		75	4				4
1.17	1^+			15						
2.66	2^-			97						
2.96	3^+		64		64	3				3
3.69	2^-	30						51		

FIG. 11. Analysis of the hybridization mechanism for antiferromagnetic MnSb in the Γ point. States for one of the spin directions. (a) Energy levels in the absence of d-d and d-p hybridization. (b) Energy levels after inclusion of d-p hybridization. (c) Calculated energy levels. Heavy lines are degenerate states.

A comparison between the hybridization schemes for AF-MnSb (Fig. 11) and those of F-MnSb (Figs. 8 and 9) leads to the following conclusions.

(1) In the case of AF-MnSb, d-d interactions lower the center-of-mass of the occupied d band. Since this effect is absent in F-MnSb, the d-d interactions favor the antiferromagnetic alignment.

(2) The p-d hybridization between Γ_5^+ states in F-MnSb and Γ_3^+ states in AF-MnSb is more effective in lowering the energy of the Γ_5^+ state at -2.20 eV of the minority-spin electrons in F-MnSb, than in lowering the energy of the Γ_3^+ state at -0.89 eV of AF-MnSb. Moreover, in AF-MnSb the energy of this state is raised by d-d interactions, while in F-MnSb d-d interactions lower the energy. These two effects result in the observed high DOS at the Fermi level for AF-MnSb (Fig. 10) and favor the ferromagnetic alignment.

(3) Covalent interactions between Mn d states in AF-MnSb, whether direct or mediated by the Sb band, lead to a lowering of the local moments: $3.16\mu_B$ in AF-MnSb versus $3.24\mu_B$ in F-MNSb. The loss of exchange energy which results from this loss of local magnetization stabilizes the ferromagnetic alignment, as described by Kübler, Williams, and Sommers.[20]

The small difference between magnetic moments of F-MnSb and AF-MnSb indicates that they can be described as localized moments. In this respect MnSb is closer to the Heusler alloys, which can be described as ideal local-moment systems,[20] than to pure Mn. In pure Mn band-structure calculations show that the moments change drastically if the type of magnetic order is changed.[21] Contrary to what is found for the Heusler alloys, in Mn metals the direct Mn-Mn interactions play an important role in the coupling of the magnetic moments. The most important coupling mechanism in MnSb is the covalent

interaction with the Sb $5p$ band. It is essential that this band is not completely filled, as covalent interactions between occupied states do not lower the total energy. This situation occurs in MnTe, which is an antiferromagnetic insulator.

IV. COMPARISON WITH EXPERIMENTAL RESULTS

When a comparison between theoretical results and experimental data is made, one must keep in mind that it is difficult to prepare homogeneous and stoichiometric MnSb. The occupation of the trigonal bipyramidal holes in the Sb sublattice by metal atoms (Fig. 2) occurs in many compounds which, for the ideal stoichiometric composition, have the NiAs structure. Most of the more alloylike compounds have a large homogeneity range and in some cases (e.g., MnSn, VSb, FeSn) the stoichiometric composition lies far outside this range. The homogeneity range of $Mn_{1+x}Sb$ is reported to extend from $x = 0.04$ to 0.15 for samples which are quenched from $700-800\,°C$ (Teramoto and van Run[34] and Bouwma[26]). Slowly cooled $Mn_{0.75}Sb$ and $Mn_{1.00}Sb$ are reported to decompose into Sb and $Mn_{1.03}Sb$.[26] The preparation of homogeneous $Mn_{1.013}Sb$ has been reported by Chen et al.[13] The question remains whether stoichiometric MnSb does exist.

Although the interpretation of experimental data for nonstoichiometric crystals is difficult, studies have been undertaken of the influence of a *variation* of excess Mn,[13] making extrapolations to the stoichiometric composition. Bouwma[26] also investigated the influence of a (partial) substitution of Sb by Sn and Te and of Mn by V, Cr, and Fe.

In this section we compare the results of our calculation with the following. (1) ground-state properties: magnetic moments, spin density, and electronic contribution to the specific heat; (2) transport properties: Hall effect and Seebeck effect; (3) excitation spectra: optical spectra and XPS.

In Sec. III it was shown that spin-orbit effects on the overall band structure are relatively small. We will not deal with effects which depend strongly on spin-orbit interaction, such as the magneto-optical effects, the anomalous Hall effect, and the magnetic anisotropy. An up-to-date review of the experimental work on MnSb is given in Ref. 35.

A. Specific heat

The major difference between our results and the model of the electronic structure proposed by Chen et al.[13] and Allen et al.[14] is the density of states at the Fermi level, $N(\epsilon_F)$ [Fig. 1(c)]. Neglecting mass-enhancement effects, by electron-phonon and electron-magnon interaction, e.g., our calculated $N(\epsilon_F)$ can be compared with the results of heat-capacity measurements.[12] From the temperature dependence of the specific heat, the electronic contribution γT was determined. The coefficient γ is related to $N(\epsilon_F)$ by[36]

$$\gamma = \frac{\pi^2}{3} k_B^2 N(\epsilon_F) \,. \tag{7}$$

Extrapolating the composition-dependent values of γ of compounds $Mn_{1+x}Sb$ to stoichiometric MnSb, a coefficient $\gamma = 2.8 \pm 0.4$ mJ mol^{-1} K^{-2} is found. Using Eq. (7) this corresponds to a value $N_{expt}(\epsilon_F) = 2.4 \pm 0.4$ states eV^{-1} (unit cell)$^{-1}$, which agrees with our calculated value of $N_{calc}(\epsilon_F) = 2.6$ states eV^{-1} (unit cell)$^{-1}$ (Table VI).

B. Magnetic moments and spin density

The band-structure calculation yields a net saturation magnetic moment of $3.24\mu_B$ per Mn atom (Table VI). From the spin density around the Mn atom there is a contribution of $3.3\mu_B$ per Mn atom, while we find a small negative spin density on the Sb sites of $-0.06\mu_B$ per Sb atom. The experimental saturation magnetic moment of stoichiometric MnSb is $3.5 \pm 0.1\mu_B$ per Mn atom. This number and its accuracy summarize the results of several authors, who have measured the saturation magnetization or have performed (spin-polarized) neutron diffraction.[3,4,13,26,34,37,38] The calculated moment is about 8% lower than the experimental one. A similar discrepancy has been found by Kübler et al.[20] who performed self-consistent ASW calculations on a series of Heusler alloys. Their calculated moments were 0–13 % smaller than the experimental values. The authors give as a possible explanation that there could be an orbital contribution to the magnetic moment, which is not included in the calculation. However, for MnSb the measured gyromagnetic ratio is 1.978 ± 0.002,[39] indicating that the orbital momentum is almost completely quenched. The problem of an underestimation of the magnetic moment which seems to be systematic in these compounds, is still to be solved.

More detailed information about the spin density has been obtained by spin-polarized neutron diffraction. Yamaguchi et al.[40] and Reimers et al.[41] have shown that the magnetic moments are strongly localized on the Mn sites. They measured pronounced deviations from a spherical spin distribution. As the Mn atom is coordinated by a trigonally distorted octahedron of Sb atoms, the charge and spin densities can be represented as a sum of densities with a^t_{1g}, e^t_g, and e_g symmetry. The orbital wave functions are ψ_{x_0}, $\psi_{x\pm}$, and $\psi_{u\pm}$, respectively:

$$\psi_{x_0} = d_{z^2} \, ,$$

$$\psi_{x\pm} = \frac{1}{\sqrt{3}}\left[[d_{x^2-y^2} \mp id_{xy}] \pm \frac{1}{\sqrt{2}}[-id_{yz} \mp d_{xz}] \right] , \quad (8)$$

$$\psi_{u\pm} = \frac{1}{\sqrt{3}}\left[\frac{1}{\sqrt{2}}[d_{x^2-y^2} \mp id_{xy}] \mp [-id_{yz} \mp d_{xz}] \right] ,$$

in the coordinate frame of Fig. 2.

In Table IX we give the calculated occupations of these orbitals, and the experimental unpaired electron occupation for $Mn_{1.05}Sb$ (Ref. 40) and $Mn_{1.09}Sn$.[41] The calculated numbers depend, of course, on the choice of a size for the Mn atom. The calculated numbers refer to the number of electrons within the Wigner-Seitz sphere. The experimental data have been fitted to a theoretical radial charge distribution for atomic Mn $3d$ states which determines the effective size of the Mn atom. For $\psi_{x\pm}$ and

TABLE IX. Calculated and experimental unpaired electron occupations of ψ_{x_0}, $\psi_{x\pm}$, and $\psi_{u\pm}$ $3d$ orbitals of Mn. The numerical accuracy of calculated values is about $\pm 5\%$.

	Calculation MnSb	Experiment $Mn_{1.05}Sb^a$	$Mn_{1.09}Sb^b$
ψ_{x_0}	$0.91 - 0.31 = 0.60$	0.89 ± 0.08	0.57 ± 0.09
$\psi_{x\pm}$	$1.81 - 0.28 = 1.53$	1.61 ± 0.12	1.60 ± 0.07
$\psi_{u\pm}$	$1.72 - 0.55 = 1.17$	1.22 ± 0.10	1.28 ± 0.06

[a]Reference 40.
[b]Reference 41.

$\psi_{u\pm}$ states the calculated unpaired electron occupation agrees with the experimental data. For ψ_{x0} states the unpaired population given by Yamaguchi et al. is significantly higher than the experimental value of Reimers and our calculated value. Yamaguchi et al. also find a spherically symmetric negative magnetic moment of $(0.20 \pm 0.13)\mu_B$ at the Sb sites. Reimers et al. have not found this negative polarization of Sb. Our calculations yield a negative moment of $-0.06\mu_B$ per Sb atom. We conclude that the calculated results are in good agreement with the experimental data of Reimers et al.

The data in Table IX give a good illustration of our analysis of the band structure at Γ (Sec. III). For the majority-spin direction the occupation of ψ_{x_0} and $\psi_{x\pm}$ states is about 90%. The $\psi_{u\pm}$ states (at Γ, Γ_5^+ e_g states) have in a nondistorted octahedral coordination of Sb atoms their largest probability on lines that connect Mn and Sb atoms. The formation of covalent Mn—Sb bonds lowers their occupation for the majority-spin direction to 86%, while it raises their occupation for the minority-spin direction to 28%. For the nonbonding $\psi_{x\pm}$ states the minority-spin occupation is only 14%. The formation of Mn—Mn covalent bonds (at Γ, Γ_1^+ state) raises the minority-spin occupation of ψ_{x_0} states to 31%. This causes a flattening of the spin-density distribution in the a-c plane, which is shown in Fig. 12. This figure can be compared directly to the experimental spin density of Rei-
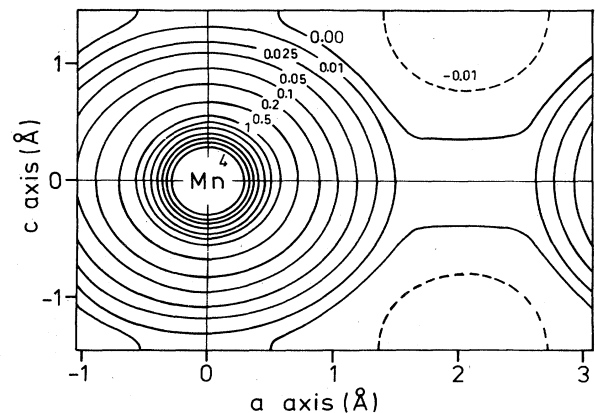

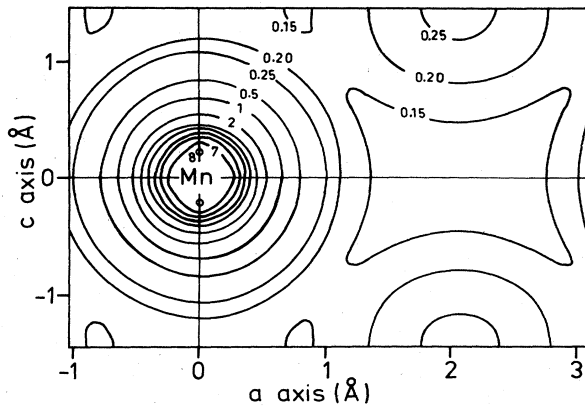FIG. 12. Calculated spin-density distribution in the a-c plane. Units: electrons/Å^3.

FIG. 13. Calculated charge-density distribution in the a-c plane. Units: electrons/Å^3.

mers *et al.* (Ref. 41, Fig. 6). The total valence electron charge density in the a-c plane is shown in Fig. 13. Charge and spin densities along the c axis are shown in Fig. 14. The calculated radial spin density agrees very well with that reported by Sirota *et al.*[42] The discrepancy at low distances from the atom is attributed to the experimental impossibility to measure very high angle reflections in neutron-diffraction experiments.

The band models proposed by Yamaguchi *et al.*[40] and Reimers *et al.*[41] which were based on assumed crystal-field splittings and bandwidths, and measured unpaired occupations of a^t_{1g}, e^t_g, and e_g bands are not in agreement with our calculation, as in these models the Mn atoms have essentially four d electrons. Our calculations explain why the observed magnetic form factors for Mn are best fit with theoretical d^{5-6} configurations of Mn.

C. Transport properties and the Fermi surface

The ordinary Hall coefficient of MnSb is positive. At room temperature Chen *et al.*[13] found from the slope of
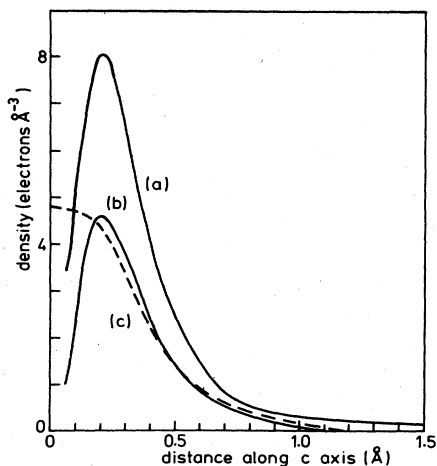
FIG. 14. (a) Radial charge density along the c axis (calculated). (b) Radial spin density along the c axis (calculated). (c) Radial spin density along the c axis (Ref. 42).

the Hall resistivity versus magnetic field above 1.6 T a value which was close to $10^{-10}\,\text{m}^3\,\text{A}^{-1}\,\text{sec}^{-1}$.

The Seebeck coefficient is negative.[13,34,43] Chen *et al.* have found a room-temperature value of $-3.5\,\mu\text{V}/°\text{C}$ for stoichiometric MnSb.

In order to be able to interpret the Hall effect and the Seebeck effect of MnSb, the Fermi surface has been calculated. In Fig. 15 the cross sections of the Fermi surface with the boundary planes of the irreducible part of the Brillouin zone are shown. The states in the shaded areas are unoccupied.

A calculation of the Hall coefficient is very complicated.[44] We will discuss the Hall effect qualitatively in terms of the Fermi-surface geometry and the wave-function character states at the Fermi surface. Sheets $14^\uparrow$ and $9^\downarrow$ clearly enclose holelike areas. The major part of the Fermi surface of band $15^\uparrow$ can also be called a hole surface. The electronic states at the surfaces are predominantly of Sb $5p$ character. The Fermi surface which originates from band $16^\uparrow$ is complicated. The electrons at the Fermi surface of band $10^\downarrow$ are predominantly of Mn $3d$ character. As the mobility of d electrons is relatively low, the contribution of this sheet to the Hall effect is probably small. The positive sign of the Hall coefficient shows that negative contributions from the electronlike parts of sheets $15^\uparrow$ and $16^\uparrow$ are more than compensated by the positive contributions from the holelike parts of the Fermi surface.

The thermoelectric power of metals can be written as

$$Q = -\frac{\pi^2 k^2 T}{3\,|\,e\,|} \left[\frac{\partial \ln \Lambda}{\partial E} + \frac{\partial \ln S}{\partial E} \right]_{E=\epsilon_F}, \tag{9}$$

where S is the Fermi-surface area, and Λ is the mean free path of the electrons. Electronlike surfaces are likely to give a negative contribution to Q due to the second term
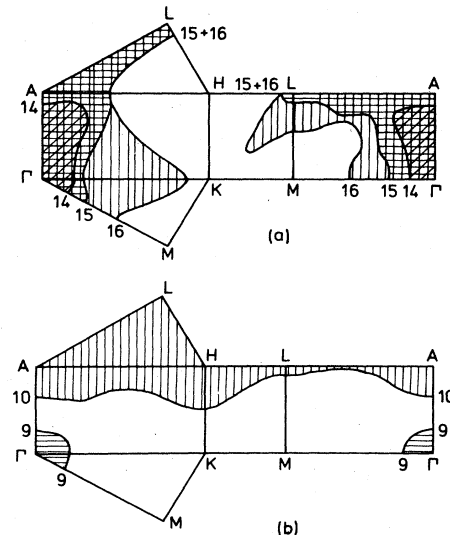

FIG. 15. Cross-sections of the Fermi surface with the boundary planes of the irreducible part of the Brillouin zone. Hole areas are shaded. (a) Majority-spin electrons. (b) Minority-spin electrons. The bands have been numbered in increasing energy order, starting with the Sb $5s$ band.

in Eq. (9). The negative sign of the Seebeck coefficient Q can be due to the first term in (9) for holelike sheets of the Fermi surface, or to electronlike sheets with low mobility which contribute little to the Hall effect (d electrons of sheets $15^\uparrow$ and $16^\uparrow$).

D. X-ray photoelectron spectroscopy

XPS measurements on $Mn_{1.01}Sb$ have been performed by Liang and Chen.[12] Their valence-band spectrum is shown in Fig. 16, together with the calculated DOS, broadened by the experimental resolution of 0.6 eV. The maximum at -2.5 eV in the spectrum corresponds to the Mn $3d^\uparrow$ peak in the DOS. The band with mainly Sb $5s$ character is clearly separated from the other bands. Its peak position at -9.7 eV is slightly lower than the maximum in the DOS at -9.0 eV.

The spectrum is probably broadened by lifetime effects. The calculated one-particle DOS and the XPS spectrum can also be different because of the effect of different cross sections and electron correlation. Partial photoionization cross sections for the valence-band electron of MnSb are tabulated in Table X. These atomic data can only be regarded as guidelines, if applied to valence states. The main conclusion is that the cross-section ratio of Sb $5p$ and Mn $3d$ states of nearly 2 may explain the relatively small contribution of the Mn $3d$ states. Since the Mn $3d^\uparrow$ band is essentially occupied, it is not expected that correlation effects will lead to satellite peaks. The occupied Mn $3d^\downarrow$ states are rather delocalized, forming covalent bonds. Therefore we do not expect large correlation effects from these states.

A more complete comparison with the calculated DOS will be possible if an inverse photoelectron spectrum [bremsstrahlung isochromat spectroscopy (BIS)] is combined with the XPS spectrum. Such experiments would make it possible to determine directly the position of the Mn $3d^\downarrow$ peak above the Fermi level.

E. Optical properties.

An analysis of the reflection spectra of $Mn_{1+x}Sb$ by Allen et al.[14] resulted in the energy-level model shown in Fig. 1(c). The low-energy region ($\hbar\omega < 1$ eV) of the optical conductivity could not be understood in terms of intraband transitions only, because a fit to a simple Drude
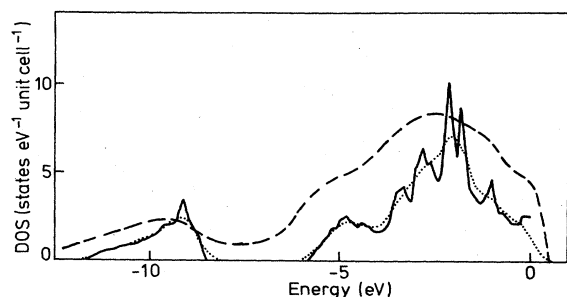
TABLE X. Calculated partial cross section per valence electron for photoemission at 1487 eV, by Scofield (Ref. 45). Electronic configuration of the gas-phase atoms are assumed. Cross sections relative to Mn $3d$.

Orbital	Cross section
Mn $3d$	1.00
Mn $4s$	1.11
Sb $5s$	2.59
Sb $5p$	1.84

expression was not possible. Therefore the authors concluded the presence of a high Mn $3d$ partial DOS at the Fermi level. We have calculated the interband contribution to the optical conductivity $\sigma(E)$ (Fig. 17), not including matrix-element effects, from the joint density of states $J(E)$:

$$\sigma(E) \propto \frac{J(E)}{E} ,$$

$$J(\hbar\omega) = \int_{\epsilon_F}^{\epsilon_F + \hbar\omega} dE\, N(E - \hbar\omega)N(E) .$$

(10)

Because $J(E)$ was calculated directly from the density of states $N(E)$, no momentum conservation was assumed. This is a reasonable approximation for MnSb at 300 K, because of the strong spin-disorder scattering. Including momentum conservation would lead to a somewhat more pronounced structure in $\sigma(E)$, although the overall behavior would not change. In Fig. 17(c) we have also drawn the experimental optical conductivity of MnSb at 300 K.[14]

Figures 17(a) and 17(b) show that even at the lowest energies there are interband transitions. The deviation from a Drude behavior must be due to these transitions. Transitions to the Mn $3d^\downarrow$ band become important above 0.5 eV. A peak is found at 2.5–3.0 eV in the experimental as well as in the theoretical spectrum, corresponding to transitions to the Mn $3d$ bands. The observed structure in the experimental optical conductivity of MnSb is very weak compared to the calculated structure in $J(E)/E$ (summed over both spin directions). This is remarkable, since in the

FIG. 16. (a) ——, calculated total density of states. (b) · · · ·, calculated DOS, broadened with a Gaussian of full width at half height=0.6 eV. (c) — — —, XPS spectrum (Ref. 12).
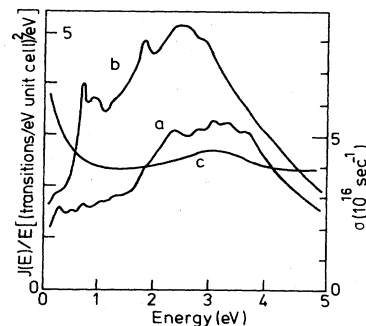

FIG. 17. Calculated function $J(E)/E$ for (a) majority-spin electron, and (b) minority-spin electrons, (c) experimental optical conductivity $\sigma(E)$ (Ref. 14).

optical conductivity of the related compound MnAs a more pronounced structure has been found.[46] This is also the case for the spectra of CrSb, NiSb, and NiAs.[14] Another surprising observation[14] for which we have no explanation is that the spectra of $Mn_{1+x}Sb$ appear to be nearly independent of x, in the range $0.013 < x < 0.15$.

F. Nonstoichiometric $Mn_{1+x}Sb$

For nonstoichiometric $Mn_{1+x}Sb$ the observed relation between the coefficient γ of the electronic contribution to the specific heat and x is[13]

$$\gamma = 2.8 + 150x \tag{11}$$

(in units of $mJ\,mol^{-1}\,K^{-2}$), for $0 < x < 0.15$. The magnetization of $Mn_{1+x}Sb$ decreases with x. Okita et al.[4] have found

$$\mu = (3.57 - 5.5x)\mu_B \tag{12}$$

per formula unit at 4.2 K. Measurements of Chen et al.[13] essentially agree with this result. It was also reported that the Curie temperature decreases with x.[4,13,37] From spin-polarized neutron diffraction it was concluded that the excess Mn atoms have no magnetic moment within the experimental error.[47]

It has been proposed that the very rapid increase of γ with x and the decrease of the magnetization could be explained in a rigid-band model.[13] According to our calculation this cannot be the case. Even at the peak in the minority DOS at $+0.5$ eV, the DOS is only a factor of 3 higher than $N(\epsilon_F)$ (Fig. 5). However, in $Mn_{1.15}Sb$ the value of γ has increased by a factor of 8 as compared to MnSb [Eq. (11)].

If the local electronic structure at the excess Mn (Mn_i) site is dominated by Mn_i-Sb interactions, as expected because of the small Mn_i-Sb nearest-neighbor distance, the magnitude of the local Mn_i moments could be strongly reduced. From the virtual bound-state model of Anderson[48] it follows that this would be the case if due to Mn_i-Sb hybridization the d-band widths are comparable to the exchange energy. This model would explain the observed absence of a magnetic moment on excess Mn. However, it would not explain the rapid increase of the density of state at the Fermi level [Eq. (11)] and the rapid decrease of the magnetization with x [Eq. (12)]. The experimental data [Eq. (11)] suggest that as a result of excess Mn atoms, a very sharp peak in the density of states is developed. This is a very interesting situation for which we have no explanation. In our view, direct or indirect Mn_i-Mn interactions could lead to a decrease of the moments of the regular Mn atoms, but not to a sharp peak in the DOS at the Fermi level.

V. CONCLUDING REMARKS

The analysis of the band-structure calculation and the experimental data has shown the importance of covalent interactions in MnSb. We have found that the total splitting of the d bands is 0.8 eV larger than the exchange splitting of 2.7 eV, the difference being caused by p-d hybridization. The d electrons are itinerant, mainly because of d-d covalent interactions along the c axis, leading to bandwidths of 1.7 and 2.1 eV for majority- and minority-spin electrons, respectively. The p-d covalency is essential for (1) the explanation of the observed magnetic moment and electronic contribution to the specific heat in terms of the DOS, (2) the discussion of the competition between ferromagnetism and antiferromagnetism in MnSb, and (3) the explanation of the observed asphericity of the magnetic moment.

As the Fermi surface is very complicated, a discussion of the Hall effect and the Seebeck effect needs a detailed knowledge of the wave-vector, energy, and temperature dependence of electron-scattering mechanisms. Finally we suggest two experiments. BIS experiments may complement the XPS data, yielding information about the unoccupied states. Optical spectroscopy, e.g., ellipsometry, as a function of temperature and stoichiometry is needed to check the remarkable lack of structure in the available reflection spectrum and the observation that the reflection spectrum does not depend on stoichiometry.

ACKNOWLEDGMENTS

[1]J. W. Allen and W. Stutius, Solid State Commun. 20, 561 (1976).

[2]H. Ido, J. Phys. Soc. Jpn. 25, 625 (1968).

[3]W. Reimers, Ph.D. thesis, University of Marburg/Lahn, 1980.

[4]T. Okita and Y. Makino, J. Phys. Soc. Jpn. 25, 120 (1968).

[5]R. A. de Groot, F. M. Mueller, P. G. van Engen, and K. H. J. Buschow, Phys. Rev. Lett. 50, 2024 (1983).

[6]P. G. van Engen, K. H. J. Buschow, R. Jongebreur, and M. Erman, Appl. Phys. Lett. 42, 202 (1983).

[7]P. G. van Engen (private communication).

[8]J. B. Goodenough, Magnetism and the Chemical Bond (Interscience, New York, 1963).

[9]W. Albers and C. Haas, Phys. Lett. (Netherlands) 8, 300 (1964).

[10]K. Bärner, Phys. Status Solidi B 84, 385 (1977).

[11]J. Bouwma and C. Haas, Phys. Status Solidi B 56, 299 (1973).

[12]K. S. Liang and T. Chen, Solid State Commun. 23, 975 (1977).

[13]Tu Chen, W. Stutius, J. W. Allen, and G. R. Steward, in Magnetism and Magnetic Materials—1975 (Philadelphia), Proceedings of the 21st Annual Conference on Magnetism and Magnetic Materials, edited by J. J. Becker, G. H. Lander, and J. J. Rhyne (AIP, New York, 1976), p. 532.

[14]J. W. Allen and J. C. Mikkelsen, Phys. Rev. B 15, 2952 (1977).

[15]L. M. Sandratskii, R. F. Egorov, and A. A. Berdyshev, Phys. Status Solidi B 103, 511 (1981).

[16]L. M. Sandratskii, R. F. Egorov, and A. A. Berdyshev, Chemical Abstracts No. 96-60297. Available from Vsesoyuznyy Institut Nauchnoy I, Tekhnisheskoy Informatsii, Baltiyskaya Ulitsa, 14, Moscow, USSR.

[17]R. Podloucky, Solid State Commun. 50, 763 (1984).

[18]C. Herring, in Magnetism, edited by G. T. Rado and H. Suhl (Academic, New York, 1966), Vol. IV.

[19]E. P. Wohlfarth, in Ferromagnetic Materials edited by E. P. Wohlfarth (North-Holland, Amsterdam, 1980), Vol. 1, p. 1.

[20]J. Kübler, A. R. Williams, and C. B. Sommers, Phys. Rev. B 28, 1745 (1983).

[21]J. Kübler, results of band-structure calculations of pure Mn and Fe (unpublished).

[22]A. R. Williams, J. Kübler, and G. D. Gelatt, Jr., Phys. Rev. B 19, 6094 (1979).

[23]M. Methfessel and J. Kübler, J. Phys. F 12, 141 (1982).

[24]U. von Barth and L. Hedin, J. Phys. C 5, 1629 (1972).

[25]R. W. G. Wyckoff, Crystal Structures, 2nd ed. (Interscience, New York, 1960), Vol. 1.

[26]J. Bouwma, Ph.D. dissertation, University of Groningen (1972).

[27]S. C. Miller and W. F. Love, Tables of Irreducible Representations of Space Groups and Corepresentations of Magnetic Space Groups (Pruettpress, Boulder, 1967).

[28]C. Herring, J. Franklin Inst. 233, 525 (1942).

[29]J. M. Tylor and J. L. Fry, Phys. Rev. B 1, 4604 (1970).

[30]J. B. Goodenough and J. A. Kafalas, Phys. Rev. 157, 389 (1967).

[31]M. Cardona, Modulation Spectroscopy (Academic, New York, 1970), p. 70.

[32]C. E. Moore, National Bureau of Standards Circular No. 467 (U.S. GPO, Washington, D.C., 1949).

[33]Intermetallic Compounds, edited by J. H. Westbrook (Wiley, New York, 1967).

[34]I. Teramoto and A. M. J. G. van Run, J. Phys. Chem. Solids 29, 347 (1968).

[35]Gmelin Handbook of Inorganic Chemistry (Springer, Berlin, 1983), System Number 56 (Manganese), Part C, Sec. 9.

[36]C. Kittel, Introduction to Solid State Physics, 5th ed. (Wiley, New York, 1976).

[37]C. Guillaud, Ann. Phys. (Paris) 4, 671 (1949).

[38]T. Hirone, S. Maeda, I. Tsubakuwa, and N. Tsuya, J. Phys. Soc. Jpn. 11, 1083 (1956).

[39]G. G. Scott, Phys. Rev. 121, 104 (1961). Measurement of gyromagnetic ratios by Einstein—de Haas experiments.

[40]Y. Yamaguchi, H. Watanabe, and T. Suzuki, J. Phys. Soc. Jpn. 45, 846 (1978).

[41]W. Reimers, E. Hellner, W. Treutmann, and P. J. Brown, J. Phys. Chem. Solids 44, 195 (1983).

[42]N. N. Sirota, E. A. Vasilyer, Phys. Status Solidi 33, K9 (1969).

[43]W. Albers and C. Haas, Proceedings of the 7th International Conference on the Physics of Semiconductors, edited by M. Hulin (Dunod, Paris, 1964), p. 1261.

[44]M. Tsuji, J. Phys. Soc. Jpn. 13, 979 (1958).

[45]J. H. Scofield, J. Electron. Spectrosc. Relat. Phenom. 8, 129 (1976).

[46]K. Bärner, R. Braunstein, and E. Chock, Phys. Status Solidi B 80, 451 (1977).

[47]Y. Yamaguchi, H. Watanabe, and T. Suzuki, J. Phys. Soc. Jpn. 41, 703 (1976).

[48]P. W. Anderson, Phys. Rev. 124, 4 (1961).